Multi-Antenna Techniques for Enabling Passive RFID Tags and Sensors at Microwave Frequencies

Matthew S. Trotter, Christopher R. Valenta, Gregory A. Koo, Blake R. Marshall, and Gregory D. Durgin
School of Electrical and Computer Engineering
Georgia Institute of Technology, Atlanta, Georgia 30332–0250
Email: mtrotter@gatech.edu, christopher.valenta@gatech.edu, gkoo3@gatech.edu,
bmarshall9@gatech.edu, durgin@gatech.edu

***Abstract*—Multi-antenna techniques are typically avoided in passive RFID because of the large footprints required. However, the smaller footprints required at microwave frequencies such as the 5.8 GHz industrial, scientific, and medical (ISM) band allow the use of multiple antennas. Two new multi-antenna technologies are featured in this paper to provide power and communications to a passive wireless tag in the 5.8 GHz ISM band. A four-layer FR-4 PCB is presented, which uses a staggered-pattern charge collector (SPCC) and a retrodirective array phase modulator (RAPM). An SPCC is an energy harvester that has two independent antenna arrays. These arrays provide increased gain and beamwidth over a single-antenna source. A RAPM backscatters the reader-transmitted signal directly back to the reader and provides quadrature phase-shift keyed (QPSK) signaling.**

I. Introduction

Recently, low-quantity passive RFID-enabled sensors have been used to monitor electric power line current in power substations [1] and warn construction workers of nearby heavy objects with SmartHat [2]. In these applications, a fabricated PCB design is chosen as opposed to an application-specific integrated circuit (ASIC) design. While an ASIC provides a smaller form factor and lower parasitics, its cost prohibits use in these low volume applications.

This paper describes how to overcome the excess path loss that RFID tags and RFID-enabled sensors experience at microwave frequencies as compared to UHF frequencies. Narrowband signals centered at 5.8 GHz experience 16 dB more path loss in a one-way link than narrowband signals centered at 915 MHz assuming a free-space path loss model. In the backscatter channel, the same narrowband signal at 5.8 GHz experiences 32 dB more path loss. Additional antenna gains can be realized to mitigate or overcome this extra path loss by using multiple antennas. Antennas at 5.8 GHz are approximately $1/6^{\text{th}}$ the size of similar 915 MHz antennas. Thus, multi-antenna configurations at 5.8 GHz can be realized in the same footprint of a single 915 MHz antenna.

The tag presented in this paper demonstrates a passive tag that operates at 5.8 GHz with a read range of 66 cm. Multiple charge pump circuits connected to antenna arrays collectively cover a broad area of space with high gain. A low-powered, reconfigurable retrodirective antenna array conveys tag data using quadrature phase-shift keyed (QPSK) digital modulation.

The first multiple-antenna technique is a staggered-pattern charge collector (SPCC), which operates as two or more independent energy harvesters. The presented SPCC uses 2 two-element antenna arrays with 2.5 dBi main antenna beams and a total 3-dB beamwidth of 114.8°. This way, the passive tag can benefit from high directivity in two different directions. SPCCs allow a passive tag to move away from the conventional single-antenna topology [3] with an omnidirectional pattern, which limits maximum directivity.

The second multiple-antenna technique is the retrodirective array phase modulator (RAPM). This technique uses an L-element antenna array to reflect the tag-received signal (from the reader) at the same angle of incidence back toward the reader with L^2 more signal power than a tag with just a single antenna. In addition, the RAPM allows high-order signaling schemes such as QPSK modulation rather than two-state schemes such as binary phase-shift keying (BPSK) or phase-interval encoding (PIE) as used in the EPCGlobal Class 1, Generation 2 standard [4]. This work demonstrates QPSK signaling using two 4-way microwave switches and two patch antennas.

In this paper, an overview of the tag design is presented first with descriptions and design methodologies for each tag system component. The test results in this paper give the maximum range, SPCC charge pump performance, and QPSK constellation.

II. Tag Design

The tag is designed to interface with a wide variety of sensors by using the ultra-low-power Texas Instruments (TI) MSP430F2013 microcontroller [5], which backscatters data at a symbol rate of 1 Msym/s. The finished tag is shown in the picture in Fig. 1 with all major system components labeled.

A block diagram of the major devices in the tag is shown in Fig. 2. The TI microcontroller is powered by the SPCC, which converts the received RF signal from the reader into DC power using 2 two-element antenna arrays each connected to its own

This research was sponsored by NSF career grant #0546955.

M. S. Trotter, C. R. Valenta, G. A. Koo (formerly), B. R. Marshall, and G. D. Durgin are with the Department of Electrical and Computer Engineering, Georgia Institute of Technology, Atlanta, GA, 30332 USA e-mail: mtrotter@gatech.edu, christopher.valenta@gatech.edu, gkoo3@gatech.edu, bmarshall9@gatech.edu, and durgin@gatech.edu.

978-1-4673-0328-6/12/$31.00 ©2012 IEEE

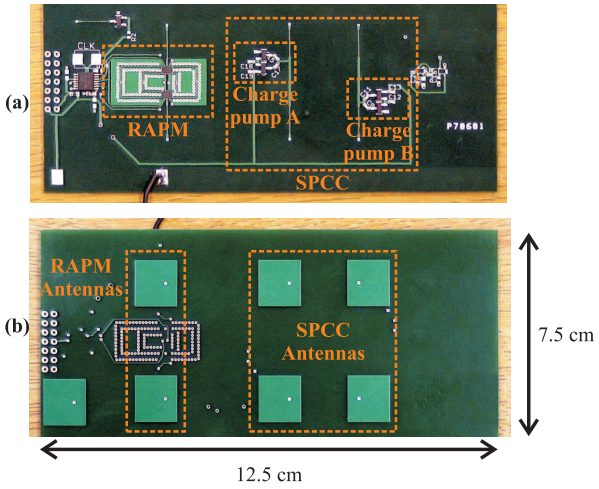

Fig. 1. The passive tag is built on a 62-mil thick FR-4 substrate. The staggered-pattern charge collector (SPCC) and retrodirective array phase modulator (RAPM) on the top side (picture a) are both connected to patch antennas on the reverse side of the PCB (picture b). The passive tag has a length of 12.5 cm and a width of 7.5 cm.

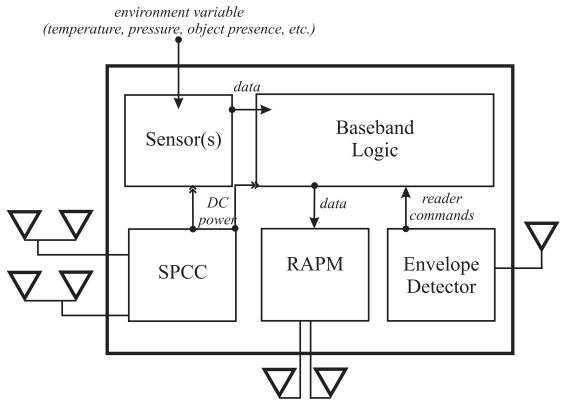

Fig. 2. A block diagram of the passive 5.8 GHz tag is shown above. A TI MSP430 microcontroller queries sensors via an ADC or USI interface. A SPCC harvests RF energy to power the microcontroller and sensors. The RAPM provides BPSK or QPSK functionality and backscatter gain. An envelope detector is sampled by the microcontroller's ADC to provide two-way communication between the reader and the tag.

4-stage charge pump. Backscatter signaling is provided by a RAPM, which signals data via QPSK.

A. Microcontroller

A TI MSP430F2013 microcontroller was chosen for this application because of its low-power operation [5]. The clock rate is 16 MHz, which requires an input current of 220 μA at 2.2 V in active mode and 0.5 μA in standby mode. This microcontroller also has the ability to incorporate both analog and digital sensors via a four-channel analog to digital converter (ADC) and an I^2C/SPI interface [5]. As shown in Fig. 2, the microcontroller links all system components. All sensors interface directly with the microcontroller where this data is encoded and parsed into packets. The packets are modulated onto the carrier waveform received from the

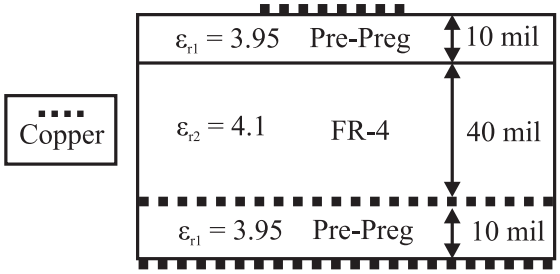

Fig. 3. The 4-layer FR-4 printed circuit board stack up used for construction of the 5.8 GHz antennas and RFID tag. Note that the pre-preg and FR-4 have different thicknesses and dielectric permittivities. The patch antennas were placed on the top layer as denoted by the dotted lines. The second layer was removed to increased the distance between the antenna and the ground plane. The third layer functioned as a ground plane. The fourth layer functioned as additional signal routing.

TABLE I
PATCH ANTENNA PARAMETERS

Parameter	Value	Method
Peak Gain	4.17 dBi	Simulated
Resonant Frequency	5.73 GHz	Measured
10dB Impedance Bandwidth	200 MHz (3.4%)	Measured
Horizontal 3dB Beamwidth	72°	Simulated
Vertical 3dB Beamwidth	104°	Simulated
Radiation Resistance	139 Ω (5.8 GHz)	Simulated
Antenna Width	1.283 cm	Designed
Antenna Length	1.165 cm	Designed

reader via the RAPM. The microcontroller can also receive data packets via an envelope detector which is sampled by the microcontroller's ADC. All of these calculations are powered by the SPCC.

B. Antennas

Half-wavelength patch antennas were chosen for this design because of their planar design and moderate gain. While dipoles would be more ideal for a purely passive RFID tag where orientation is unknown, patch antennas provide additional gains which can assist in enhancing the range of the RF tag when orientation is pre-defined.

Seven identical copies of this 50 Ω patch antenna were used in the prototype tag as seen in Fig. 1. The coaxially fed patch antennas were printed on a 4-layer FR-4 printed circuit board using the top layer for the antenna and the third layer as a ground plane as shown in Fig. 3. Since the antenna is separated from the ground plane by two different materials, a measurement and optimization procedure was completed in HFSS in order to maximize the gain and resonance. This optimization procedure is outlined in [6]. The radiation pattern of the antenna and additional parameters are found in Fig. 4 and Table I.

C. Staggered-Pattern Charge Collector

For many passive RFID tags, the processing capabilities and maximum range are limited by the amount of DC power available at the output of the charge pump. Charge pump efficiency is inherently limited by the diode threshold voltage.

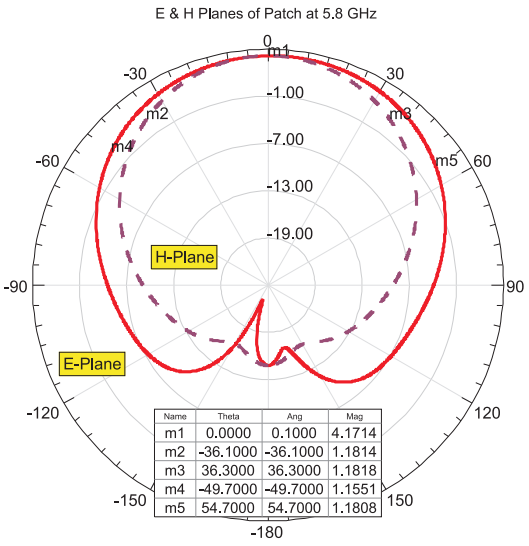

Fig. 4. Simulated E and H planes for a single patch antenna at 5.8 GHz. The maximum gain on the broad side is 4.2 dBi, and the 3-dB beamwidth is 72°.

In addition, the reader-to-tag path loss at a constant range is increased by a factor of 40 or 16 dB at 5.8 GHz as compared to 915 MHz assuming $1/r^2$ free-space path loss. The staggered-pattern charge collector (SPCC) designed in this work provides a set of 2 two-element antenna arrays. Each two-element antenna array is composed of two patch antennas feeding a single charge pump.

Traditionally, gain and half-power beamwidth are direct trade-offs in antenna theory, so as the gain of the antenna increases, it becomes more difficult to orient the tag antenna pattern toward the reader [7]. This concept applies for a single array in an SPCC. However, this tradeoff is mitigated by using a second array offset at a different angle as shown in Fig. 5. The solid plot shows a two-element linear patch array separated by a half-wavelength with a feed phase-shift of 30°, and the combination of the solid and dashed plots shows the pattern of 2 two-element arrays pointing in different directions.

The SPCC improves the tag's energy harvesting capability in two ways: First, each two-element patch array feeding a charge pump has increased gain in the main lobe over a single patch antenna feeding the same charge pump. Second, the energy harvester benefits from two main beams provided by a set of two of these two-element patch arrays. This increases the likelihood that the charge pump will receive a large amount of RF power over all possible tag orientations.

Fig. 6 shows the SPCC layout. Array A uses a feed phase difference Φ to steer its main beam at an angle θ to the left. Array B is a mirror opposite of array A, thus it has the opposite feed phase difference $-\Phi$ to steer its main beam an angle θ to the right. The feed phase difference is created by using different feed lengths to each antenna denoted x_1 and x_2.

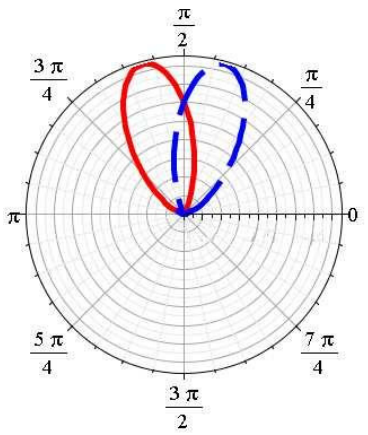

Fig. 5. The gain pattern of single two-element linear array (red solid pattern) with a 30° feed phase-shift from center compared to 2 two-element arrays with offset patterns (red solid pattern plus blue dashed pattern).

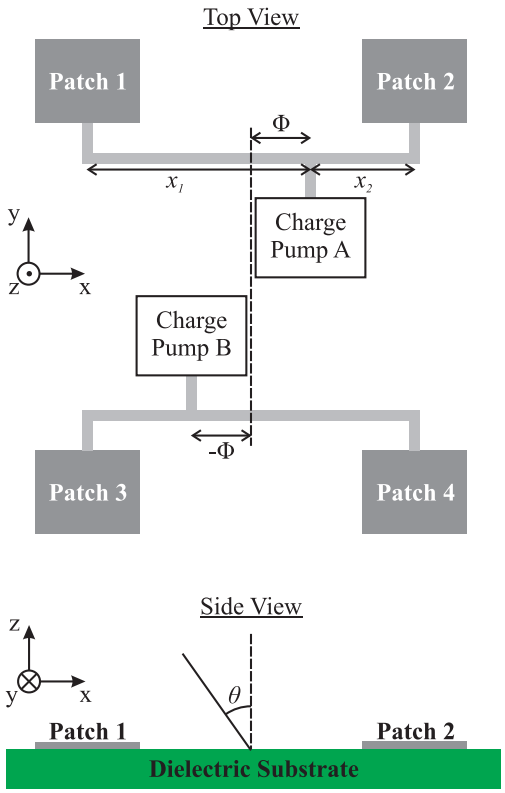

Fig. 6. The layout of the SPCC used in this work. The difference between feed-point distances x_1 and x_2 control the direction of the main lobe θ of the two-element patch antenna array.

The design equations for feed distances x_1 and x_2 are

$$x_1 + x_2 = \frac{\lambda}{2} \quad (1)$$

$$\frac{2\pi f}{v_p}(x_1 - x_2) = \Phi. \quad (2)$$

The parameters for this work are: relative permittivity $\epsilon_r =$

3.9, on-board wavelength $\lambda = 2.62$ cm, frequency $f = 5.8$ GHz, and on-board velocity of propagation $v_{\mathrm{p}} = 1.518 \cdot 10^8$ m/s. A phase difference Φ of approximately 60° on each antenna array is optimal for gain and coverage for patch antennas at 5.8 GHz [8]. Solving these equations results the length offsets to be 8.7 mm and 4.4 mm which can also be used for the array B with the offset in the opposite direction.

For the tag designed in this work, the offset lengths are 0.98 mm and 12.38 mm which correlates to a phase shift of 156°. The phase shift of 156° results in a gap or missing coverage between the two array's gain patterns which is not ideal, but the results obtained from this measurement are equally valid. The wide phase shift of 156° was originally chosen to obtain a large beamwidth.

The SPCC used in this work is simulated to show how its pattern compares with a single patch antenna. The simulations are performed in CST Microwave Studio and are shown in Fig. 7. The figure shows gain patterns from a single patch antenna, a single two-element array, and the staggered pattern array used in this work. The single patch antenna has a peak gain of 6.9 dBi and a half-power beamwidth of 81.5° while the simple array has a peak gain of 9.9 dBi but a greatly reduced half-power beamwidth at 48°. By using the staggered pattern array, a peak gain of 2.5 dBi is achieved in addition to two 3-dB beamwidths of 57.4° making the total 3-dB beamwidth 114.8°. This SPCC has a reduced maximum gain as simulated, but it is more omnidirectional than a single patch antenna.

The novelty of this simple two array set up (as opposed to a three-array or four-array set up) is the simple optimization of the offset between the two arrays by maximizing the product of power conversion gain and beamwidth. A phase shift of at least 60° between the elements on each array is optimal to ensure full utilization of the two arrays [8]. The optimality of a SPCC is based on power conversion gain and power conversion beamwidth. The power conversion gain is the maximum gain of the SPCC or, equivalently, the maximum gain of one of the two-element patch antenna arrays. The power conversion beamwidth is the 3-dB beamwidth of the complete antenna array pattern including both two-element antenna arrays.

The optimally spaced SPCC with a feed phase difference of 60° is simulated to show how it improves the gain of the antenna system without limiting coverage. Fig. 8 shows a peak gain of 8.1 dBi in addition to a wide beamwidth of 101.2°. This optimally spaced SPCC increases both the power conversion gain and the power conversion beamwidth over a single patch antenna.

D. Retrodirective Array Phase Modulator

The retrodirective array (RA) designed by Van Atta in 1959 holds the unique property that any impinging electromagnetic wave is reflected back toward the direction from which it came [9] thus reducing the power radiated in other directions. The RA accomplishes this without the use of active components and instead uses symmetry and antenna feed length restrictions. Retrodirective arrays are ideally suited for RFID tags due to this passive operation and the inherent link margin gains.

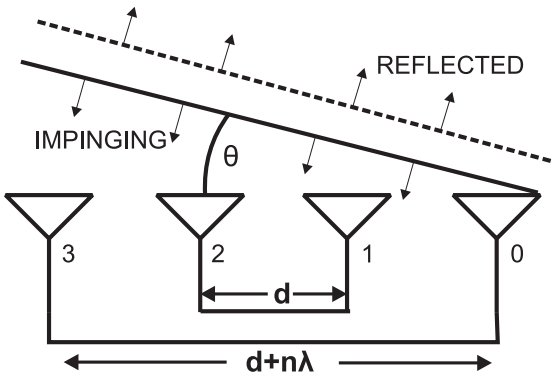

Fig. 9. A four element retrodirective array is shown. As the impinging wave comes into contact with antenna 0, the energy is coupled into the feed structure before it is reradiated through antenna 3 at a phase delay equal to the length of the feed structure between antennas 0 and 3. The same mechanism governs the operation of antennas 1 and 2.

As shown in Fig. 9, a waveform reflects back toward the source with the original angle of incidence. The transmission lines connecting each of the identical antennas in the pair have length d or $d + n\lambda$. The time-lapse diagram in Fig. 10 shows the basic operation of the RA. In frame 1, the impinging plane wave first encounters antenna 1. Some of wave energy is coupled into the transmission line which propagates towards antenna 2. In frame 2, the impinging wave has continued to propagate until it reaches antenna 2. Energy is coupled into antenna 2 and propagates in-line towards antenna 1. Meanwhile, the wave energy that entered antenna 1 has further propagated toward antenna 2. In frame 3, the impinging wave has passed and the forward propagating wave on the transmission line received by antenna 1 is about to be re-radiated by antenna 2. The propagating wave received by antenna 2 will be re-radiated by antenna 1 at a time proportional to the delay at which is was received. Finally in frame 4, antenna 2 has re-radiated the wave and antenna 1 is about to re-radiate the wave on the transmission line. Although all antennas will radiate in all directions according to their gain pattern, the sum of their patterns will coherently add in phase in the same direction from which the impinging pattern propagated. Other directions will incur destructive interference of the waves from antenna 1 and antenna 2.

An RA with two or more sets of two-element arrays can operate equivalently with lengths $d + n\lambda$ where n is a positive integer. Of course, any length between the two antennas will operate with retrodirectivity. A group of two-element arrays provides additional gain for the reflected wave toward the original direction. RAs with two or more sets can have arbitrary lengths as well. Here, the independent two-element arrays contribute constructively to the returned signal in the impinging direction, but the destructive interference in other directions is not as strong.

RAs consisting of L antenna elements provide L^2 more

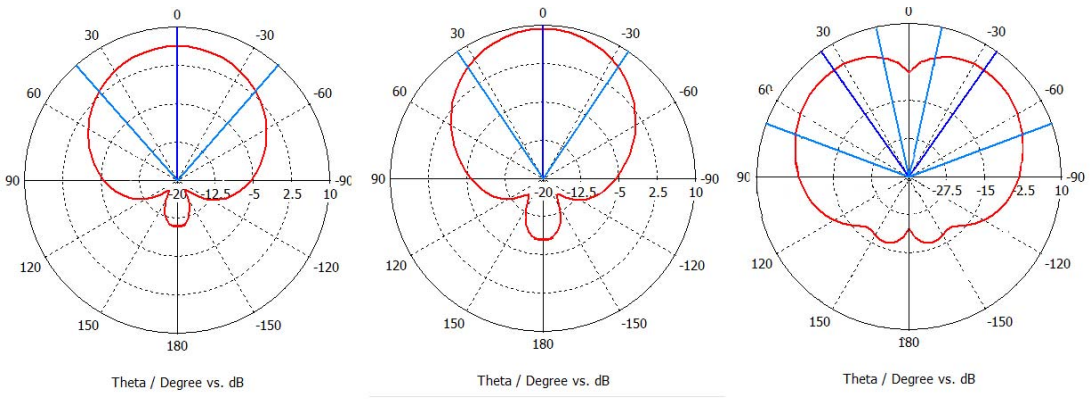

Fig. 7. Gain Patterns of a single patch antenna (left plot), two-element patch array (center plot), and a the staggered-pattern patch array used in this work with a feed phase difference of $\Phi = 156°$ (right plot).

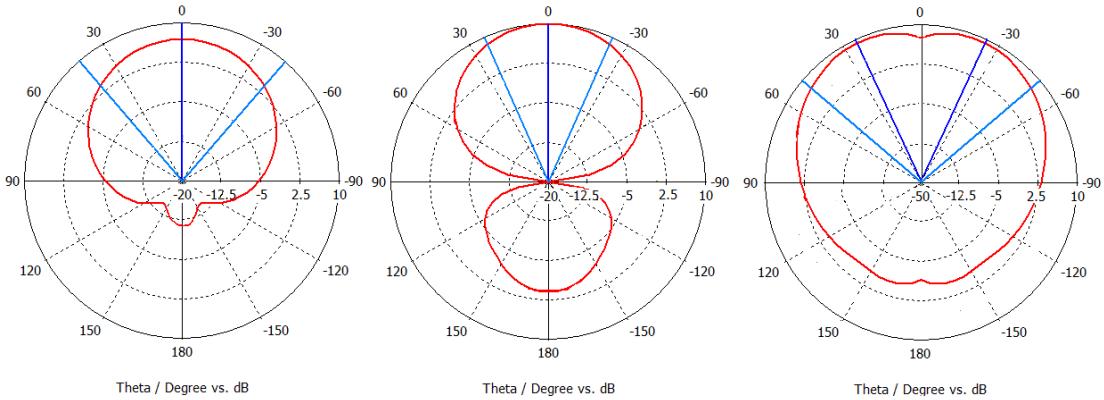

Fig. 8. Gain Patterns of a single patch antenna (left plot), two-element patch array (center plot), and a staggered-pattern patch array with an optimal feed phase difference of $\Phi = 60°$ (right plot).

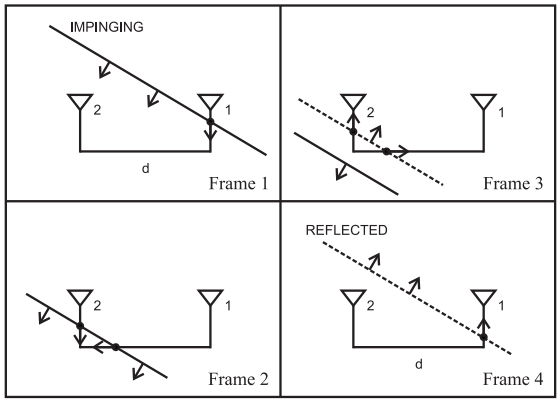

Fig. 10. A time-laps diagram showing the operation of a dual antenna retrodirective array.

backscattered power than a single antenna. It was shown that higher order PSK modulation schemes are possible using a retrodirective array [6]. By using higher order PSK modulation schemes, a higher number of bits per symbol can be transmitted which can reduce the period of time the tag's oscillator is on and thus reduce its power consumption and improve range. This can be compared to a work such as [10], which implements QAM backscatter to reduce the tag's microcontroller operation time.

A RAPM modulates data by changing the phase of the re-radiated wavefront. This is accomplished by connecting transmission lines of length $d + n\lambda/M$ between antennas for M-ary PSK (e.g. M=4 for QPSK). By varying the integer n, the re-radiated waveform will have a phase proportional to the length of the transmission line which it passed through.

The tag constructed in this work uses two patch antennas, which are identical to the antennas used in the SPCC. Each is connected to a single pole, four throw (SP4T) Hittite HMC345LP3 GaAs switch [11] in order to implement QPSK modulation. The four switching states of the switches are connected through coplanar waveguides (50 Ω characteristic impedance, 11 mil trace width, 9 mil gap) of length $\lambda/4$, $\lambda/2$, $3\lambda/4$, and λ to each other as shown in Fig. 11. Each of these four waveguides have electrical lengths that are separated by 90°. Coplanar waveguides were chosen over microstrip lines

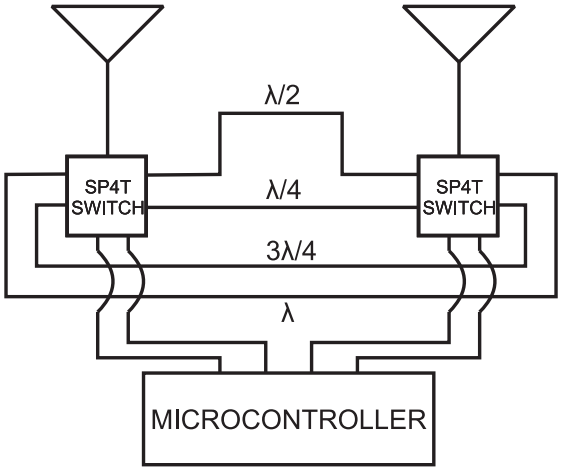

Fig. 11. A block diagram of the two element RAPM constructed on the discussed RFID tag. Transmission lines of lengths $\lambda/4$, $\lambda/2$, $3\lambda/4$, and $\lambda/4$ are feasible to be constructed because the wavelength at 5.8 GHz is 5.17cm in freespace and even less in a dielectric. Taken from [6].

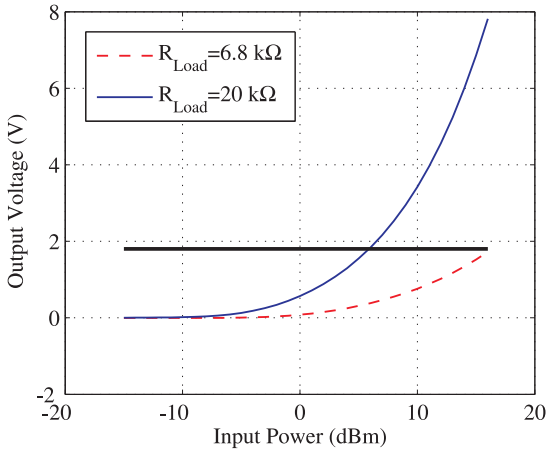

Fig. 12. Measured 4-Stage Dickson charge pump output voltage for two different load resistances. The TI MSP430F2013 presents a 10 kΩ load to the SPCC. Adapted from [12]

because they offered greater isolation between each of the four switching states. These switches are controlled by the MSP430 microcontroller.

III. Tag Testing Results

This section summarizes the tests on read range and the backscattered QPSK signal constellation.

A. Maximum Range

The maximum range of the tag is measured as 66 cm. Beyond this range, the reader could not receive any data from the tag. The reader-received tag signal has a high SNR when measured at a range of 66 cm. The signal abruplty stops when the tag is taken beyond this maximum range. Thus, the range is limited in the forward link by the energy-harversting efficiency as expected. This range is not as long as expected and can be increased by reducing the phase difference between the SPCC antennas.

The reader used to communicate with the tag is a bistatic transceiver operating at a center frequency of 5.8 GHz. Identical 4-element patch antenna arrays with a maximum broadside gain of 8 dBi are placed side-by-side facing toward the tag in the environment. The average transmitted power is 30 dBm.

Rotating the tag from -90° to +90° with respect to the reader antennas qualitatively shows wide-angle operation when measured at a 60 cm range. The tag does not respond when the broadside of the SPCC faces the broadsides of the bistatic reader antennas. This agrees well with the simulated SPCC pattern in the right plot of Fig. 7, which shows a dip in the pattern at $\Theta = 0°$ (broadside). Also, the tag does not respond within a few degrees of the rotational extremities (-90° or +90°).

B. SPCC Charge Pumps

One of the 4-stage charge pumps from the SPCC is measured comprehensively across different resistive loads and different input frequencies in [12]. This charge pump uses Avago HSMS2862 diodes with a 350 mV threshold voltage [13] and 10 pF RF capacitors all connected by 50 Ω microstrip lines at 5.8 GHz. Fig. 12 shows the output voltage of the charge pump for a range of RF input power and two different load resistors. Of all the measured load resistors, these loads shown are the closest to the input resistance of the TI MSP430 microcontroller when working at a clock rate of 1 MHz. The figure shows that an input power of 6 dBm or greater is required to provide the minimum 1.8 V necessary to run the microcontroller continuously.

This data suggests that the matching between the charge pumps and SPCC antennas can be improved. The input impedance to a charge pump varies with input power, but matching strategies have been shown to improve the power efficiency of charge pumps [14].

C. RAPM Constellation

The RAPM's signal constellation is measured at a distance of 60 cm and the real and imaginary components of the reader-received signal are plotted in Fig. 13. The reader-received signal is downconverted to baseband using the homodyne receiver discussed in [15] and sampled with an Exacq CH-3150, two-channel, 12-bit analog-to-digital converter (ADC). The ADC is set to a sampling rate of 20 MHz and a capture window of 10 ms. The RAPM is programmed to alternate states sequentially at a rate of 1 Msym/sec. Table II contains the magnitude and phases of the signal constellation.

The deviations in relative phases are due to phase offsets in the switch and variations in the dielectric constant in the FR-4 substrate depending on what direction the trace is directed (parallel or perpendicular to the grain). The differences in amplitude of each constellation point can be attributed to the dielectric losses associated with the additional length of the microstrip lines. However, the figure illustrates that higher

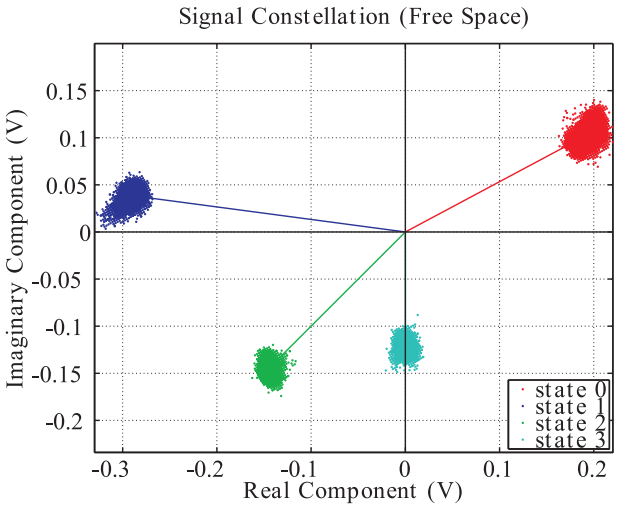

Fig. 13. The measured RAPM backscatter QPSK signal constellation shows warping due to inconsistencies in the FR4 substrate and phase offsets in the SP4T switches.

TABLE II
FREE SPACE BACKSCATTER SIGNAL PROPERTIES OF A RAPM.

State	Magnitude	Phase	Phase Difference Between States
State 0	0.22 V	28.1°	(1-0) 144.3°
State 1	0.29 V	172.4°	(2-1) 52.6°
State 2	0.20 V	225.0°	(3-2) 45.0°
State 3	0.12 V	270.1°	(0-3) 118.3°

order signal constellations are possible with RAPMs. The errors discussed can be corrected by characterizing the RF switch and revising the trace routings of the RAPM.

IV. Future Work

Future revisions will include a characterization of SP4T RF switches. The phase differences between the RF port and the four switching ports will be measured so that the relative phase difference between states in the QPSK constellation can be calibrated to be 90°. Additionally, an improved SPCC with optimal power conversion gain and bandwidth will be implemented along with a more efficient charge pump.

Charge banking will also be investigated. Charge banking is a technique that uses a super capacitor to store energy which is slowly charged using a charge pump. The super capacitor adds the capability for the tag to use power when there is no RF signal available from the reader.

V. Conclusions

Two multi-antenna techniques are showcased, which enable improved passive tag operation at 5.8 GHz. First, a staggered-pattern charge collector uses an antenna feed structure that allows a broader beamwidth and higher maximum gain than a single-antenna feed using a single charge pump. A staggered-pattern charge collector with 2 two-element patch antenna arrays shows a simulated 3-dB beamwidth increase of 33.3° over a single patch antenna. Second, a retrodirective array phase modulator enables digital communication of QPSK signaling of tag data and reflects incoming RF signals from the reader back toward the reader in the originating direction.

Tests and simulations showed that communicating with a passive tag built on a PCB is possible even with 32 dB extra path loss in the forward and backscatter links together. Integrated circuit designs may further improve performance and reduce manufacturing costs over a PCB design. However, for applications such as the SmartHat [2] that use PCB designs, multiple-antenna techniques improve the range and reliability of communications with a passive tag.

References

[1] C. Valenta, P. Graf, M. Trotter, G. Koo, G. Durgin, and B. Schafer, "Backscatter channel measurements at 5.8 ghz across high-voltage corona," in *IEEE Sensors Conference*, November 2010, p. 2400.

[2] S. Thomas, J. Teizer, and M. Reynolds, "SmartHat: A battery-free worker safety device employing passive UHF RFID technology," in *IEEE International Conference on RFID*, 2011, p. 85.

[3] S. L. Chen, K. H. Lin, and R. Mittra, "Miniature and near-3D omnidirectional radiation pattern RFID tag antenna design," *IEEE Electronics Letters*, p. 923, August 2009.

[4] EPCglobal, *EPC (TM) Radio-Frequency Identity Protocols Class-1 Generation-2 UHF RFID Protocol for Communications at 860 MHz - 960 MHz Version 1.2.0*, October 2008.

[5] *TIMSP430F20x3 Datasheet, Revision H*, Texas Instruments, http://www.ti.com/, August 2011.

[6] G. A. Koo, "Signal constellations of a retrodirective array phase modulator," Master's thesis, Georgia Institute of Technology, May 2011.

[7] C. Balanis, *Antenna Theory: Analysis and Design*. John Wiley & Sons, 1997.

[8] B. Marshall, "A methodology for designing stagged pattern charge collectors," Master's thesis, Georgia Institute of Technology, 2011.

[9] L. Van Atta, "Electromagnetic reflector," U.S. Patent 2,908,002, October 1959.

[10] S. Thomas and M. Reynolds, "QAM Backscatter for Passive UHF RFID Tags," in *IEEE International Conference on RFID*, 2010, pp. 210–214.

[11] *Hittite HMC345LP Datasheet*, v04.0905 ed.

[12] L. Blanca, J. Block, M. Almada, J. Gonzalez, C. R. Valenta, and G. D. Durgin, "Characterization of a 5.8 ghz 4-stage dickson charge pump with resistive loads," *The Georgia Tech Tower. (Submitted for Publication)*, 2012.

[13] *HSMS-280x, Surface Mount RF Schottky Barrier Diodes*, Avago Technologies, http://www.avagotech.com/, April 2010.

[14] K. Finkenzeller, *RFID Handbook: Fundamentals and Applications in Contactless Smart Cards and Identification*. John Wiley and Sons, 2003.

[15] J. D. Griffin, "High-frequency modulated-backscatter communication using multiple antennas," Ph.D. dissertation, Georgia Institute of Technology, March 2009.